Computing the Longtime Behaviour of NMR Propagators in Porous Media Using a Pore Network Random Walk Model

Valentin Guillon · Daniela Bauer · Marc Fleury · Marie-Christine Néel

Abstract We present a pore network model combined with a random walk algorithm allowing the simulation of molecular displacement distributions in porous media as measured by NMR. A particular feature of this technique is the ability to probe the time evolution of these distributions. The objective is to predict the displacement behaviour for time intervals larger than the experimental observation time and explore the asymptotic dispersion regime at long times. Starting from 3D micro-CT images, we computed the variance of displacement distributions of water molecules in a Fontainebleau sand and found very good agreement of the time evolution of the variance with experimental data, without fitting parameter. The model confirms a weak superdispersion in the asymptotic regime. In addition, we conclude that, since pore network models do not take into account small scale features of the porous medium (e.g., surface roughness and grain shape), the origin of the observed superdispersion is mainly due to the topology and geometry of the porous medium.

Keywords Pore network model · Random walk · NMR · Superdispersion · Porous media

1 Introduction

Classical Gaussian dispersion in porous media is characterized by a linear time dependence of the displacement variance, that is generally used to investigate molecular motion. Furthermore, macroscale models implemented in fluid dynamic or reservoir simulators are generally based on Gaussian dispersion. However, some measurements show a non-linear time dependence (Scheven et al. 2005). Commonly, the variance is written as a function of time, given by

V. Guillon · D. Bauer (✉) · M. Fleury
IFP Energies Nouvelles, 92852 Rueil-Malmaison, France
e-mail: daniela.bauer@ifpen.fr

M.-C. Néel
Université d'Avignon et des Pays de Vaucluse, UMR 1114 EMMAH,
84018 Avignon Cedex, France

$$\sigma^2 \propto t^{\alpha}. \tag{1}$$

If $\alpha = 1$, dispersion follows a classical Gaussian law. For $\alpha > 1$, the rate of growth of the variance is higher and transport is super-dispersive, whereas for $\alpha < 1$ the rate is lower and the transport becomes sub-dispersive (Metzler and Klafter 2000). Non-Gaussian dispersion can be observed in the pre-asymptotic and in the asymptotic regime. In the asymptotic regime the mean displacement $< \xi >$ is large in comparison to the average grain size d_g and mechanical dispersion has reached a steady state. In addition, particles or molecules explore a certain number of streamlines due to molecular diffusion (Scheven and Sen 2002). Anomalous dispersion is referred as non-Gaussian dispersion in the asymptotic regime. It can be observed in heterogeneous (Levy and Berkowitz 2003; Benson et al. 2000) and partially saturated homogeneous porous media (Guillon et al. 2013; Padilla et al. 1999), but even in homogeneous saturated porous media (Levy and Berkowitz 2003; Li et al. 2006). Investigating anomalous dispersion in porous media is therefore a crucial task in very different domains as contaminant hydrology, geophysics, or engineering. In this article we focus on transport in homogeneous structures, that is still often believed to be normal (displacements of individual molecules follow a Gaussian distribution) and modelled by the classical advection–diffusion equation. However, although deviation from Gaussian dispersion is weak in homogeneous structures, in some circumstances it cannot be neglected. Important issues that can be cited, are for example underground waste storage facilities. Considering the environmental impact, an accurate description of mass transport in such media, even at low concentration, becomes very important considering toxic tracers, released from industrial and agricultural waste.

Dispersion can be studied by investigating breakthrough curves of tracer experiments in columns (see Sahimi (2011) for an extended review). Another method is to observe by NMR the molecular displacement inside a specific region in a column as a function of time. In this way, time dependence of dispersion can be investigated and the exponent α precisely evaluated in a robust way. The NMR propagator technique is based on the spatial encoding of water molecules without the need for tracer particles. It was applied to homogeneous bead and sand packs (Lebon et al. 1996, 1997; Tessier et al. 1997; Seymour and Callaghan 1997; Manz et al. 1999) and the transition from the pre-asymptotic to the asymptotic regime was observed (Manz et al. 1999; Scheven and Sen 2002; Scheven et al. 2008). However, a key aspect for deriving dispersion from such experiments is to reach the asymptotic regime. Scheven and Sen (2002) reported that, in grain packs, the asymptotic regime is reached if $< \xi >> 10d_g$ and $L_d = \sqrt{2D_m t} > 0.3d_g$, where D_m is the molecular diffusion coefficient. In this case, skewness of the displacement distribution becomes zero and the distribution Gaussian. However, these conditions may yield technical difficulties since NMR observation times are limited to about $1s$ for most permeable porous media (100 to 1,000 mD). Hence, flow rates may have to be large to obey $< \xi >> 10d_g$, yielding high pressure and therefore necessitating appropriate flooding equipment. Thus, in some situations it might be necessary to extend the observation time domain by means of an appropriate model. We therefore propose in this article a pore network model (PNM) allowing the simulation of the molecular displacements being the basis of NMR experiments for observation times higher than the ones possible by NMR experiments.

PNM presents an efficient tool to study microscale physics in relatively large systems at low computation times, compared to other methods such as Lattice–Boltzmann, finite differences, volumes, or elements [see Blunt (2001) for an extended review on PNM]. Whereas the latter take into account the real pore structure, PNM uses a simplified representation of the pore space by a three-dimensional network of pore bodies interconnected by channels that correspond to the topological restrictions (constrictions). The network topology can

either be stochastically created, if only pore- and throat-size distributions are available or determined from micro-CT images. Low Reynolds number Stokes flow is simulated by solving Poiseuille's equation in a set of interconnected tubes. Dispersion is then modelled by a random walk algorithm displacing walkers inside the tubes. This type of model has been extensively used to simulate tracer transport and breakthrough curves and to compute the dispersion coefficient (e.g., Sahimi et al. (1986), Bodin et al. (2007), Koehne et al. (2011)). However, only little work is done on the simulation of the displacement distribution measured by NMR (Damion et al. 2000; Lebon et al. 1997; Zhao et al. 2010; Bijeljic et al. 2013a, Bijeljic et al. 2013b).

Lebon et al. (1997) simulated the displacement distribution in a homogeneous bead packing using a stochastically created network. They reproduced qualitatively the experimental propagators for different regimes. Zhao et al. (2010) reconstructed a network from micro-CT images of a heterogeneous carbonate and simulated the displacement distribution. Very good results in comparison to the experimental data were obtained. Damion et al. (2000) were principally interested in the simulation of propagators in two-phase condition.

The objective of this article is to present a pore network random walk model to simulate molecular displacements in a porous structure obtained from micro-CT images for observation times higher than those possible by NMR. To this goal, we simulate displacement distributions of water molecules in a sand pack for a large range of observation times and compare them to the available experimental data in order to validate the model. We then evaluate the longtime behaviour and determine the dispersion type.

2 Experiments: NMR Measurements and Sample Characteristics

The NMR technique was used to measure displacements of water molecules in a grain pack and we briefly recall here the basic principles of the method. The investigated volume, a thin slice $\mathcal{S}$ of the column located at mid-height, is submitted to a constant magnetic field B_0 generated by two permanent magnets. A magnetization is created in the slice by sending a selective excitation pulse at the Larmor frequency (20 MHz) using the NMR antenna (in this case a solenoid). After this pulse, the magnetization M in the sample is $M_0 = e^{-i\phi(t)}$, precessing around B_0 at the Larmor frequency. To encode the positions of the spin bearer molecules in a similar way as in imaging techniques, two opposite gradient pulses at time t_1 and t_2 are used, such that the magnetic field during a gradient pulse seen by a water molecule at a location $\mathbf{r}$ is $B = B_0 + \mathbf{g} \cdot \mathbf{r}$. As a result, after the first gradient pulse, the magnetization M has a phase depending on the location, $\phi = \gamma \delta \mathbf{g} \cdot \mathbf{r}$, where δ is the duration of the gradient pulse ($\delta << t_2 - t_1$) and γ is the proton's giromagnetic ratio. The second opposite pulse with direction $-\mathbf{g}$ and for the same water molecule now at position $\mathbf{r}'$ generates a net phase change $\phi = \gamma \delta \mathbf{g} \cdot (\mathbf{r} - \mathbf{r}')$. In this situation, the gradient direction is chosen parallel to the axis of the column in order to analyze the displacements of water molecules along the mean flow direction. Noting $q = \gamma \delta g$ with g being the amplitude of the gradient pulse, the magnetization from all molecules present in the slice is then

$$M(q,t) = M_0 \int P(x,t) e^{-iqx} dx \tag{2}$$

where x is the displacement during the time interval $t_\Delta = t_2 - t_1$ and $P(x,t)$ the displacement probability (propagator). In practice, the signal M is recorded for a set of g values at a fixed time interval, and this is repeated for other values of t_Δ. The variance of the displacements σ^2 is obtained directly using a short q expansion of the magnitude of the signal:

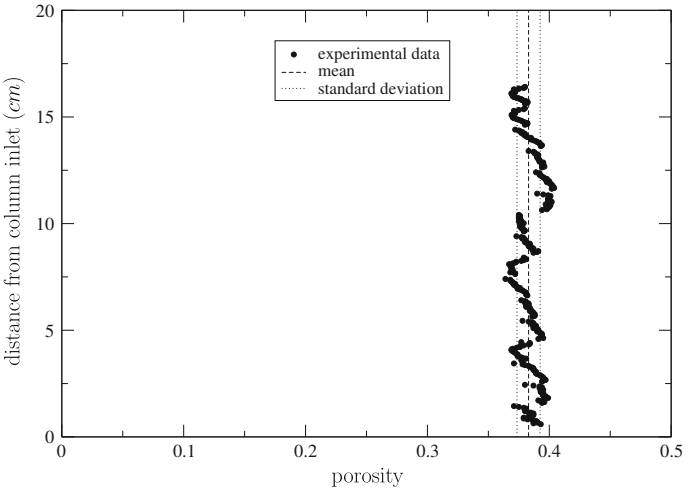

Fig. 1 Porosity profile of the sand pack measured by NMR. The average porosity is 38.3 % with a standard deviation of 0.095 %. Each point corresponds to a slice of 0.4 mm

$$\ln|M(q,t)| = -\frac{1}{2}\sigma^2 q^2$$

as described in Guillon et al. (2013).

The grain pack was built using a well-sorted Fontainebleau sand with an average grain size of 82 µm (16 % of the grains are larger than 96 µm or smaller than 69 µm). Packing in the NMR column resulted in an average porosity of 38.3 % with a standard deviation of 0.095 % (Fig. 1). Each point in Fig. 1 corresponds to a slice of 0.4 mm. This type of sand allows on one hand a good quality of the image reconstruction of the pore space. On the other hand, its grains are sufficiently small in order to permit the observation of the asymptotic behaviour by NMR.

3 Random Walk Model

3.1 Network Construction Based on Micro-CT Imaging and Flow-Field Compution

Network Construction In order to build the network the Fontainebleau sand was imaged using computer microtomography (Nanotom from GE sensing and inspection Technologies). To this goal the sand is packed in a small cylindrical tube 5 mm in diameter that can be placed inside the microtomograph. The sand pack is then imaged with a resolution of 3.5 µm. The acquired grey level image is submitted to a segmentation procedure that applies a threshold at the minimum interpeak of the grey level histogram of the image. Voxel belong either to the solid, or to the void space and the output of the segmentation procedure is then a binary image. The following pore network extraction procedure partitions the resolved pore space into individual pore volumes separated by throat surfaces. The extraction is processed in three steps: skeletonisation, pore space partitioning, and parameter calculation. The skeleton algorithm applied to the binary image is a hybrid algorithm combining thinning and distance map-based techniques called distance ordered homotopic thinning (Pudney 1998). Pores are individualized and characterized by their volumes. The

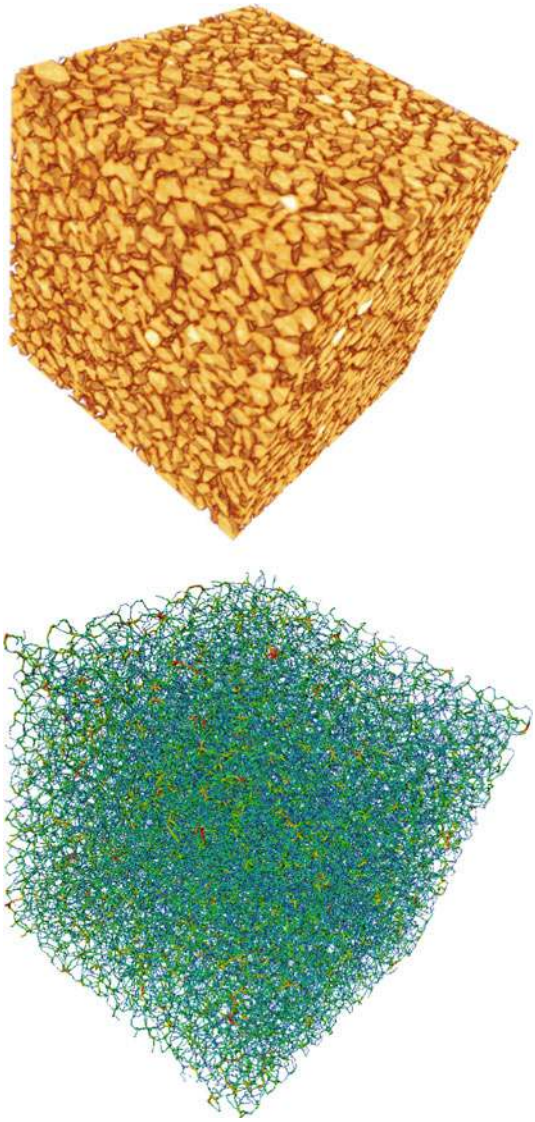

Fig. 2 Porous structure of the sandpack obtained by micro-CT imaging (*Top*), reconstructed network (*Bottom*)

pore volume intersections define the throat surfaces. The network consists then of nodes, situated in the barycenter of the pores, interconnected with cylindrical channels. The channel diameter is computed from the throat dimension by $d = 4\frac{A}{P}$ where A is the throat surface area and P its perimeter. For more detail on the pore network extraction procedure see Bauer et al. (2011).

The imaged volume has a size of $1,575^3\,\mu\text{m}^3$ resulting in a network of 10,185 pores and 25,522 channels. Figure 2 presents the pore structure as well as the reconstructed network. The following average values characterize the network: pore diameter: $\bar{D} = 60.1\,\mu\text{m}$, channel diameter: $\bar{d} = 24.4\,\mu\text{m}$, node to node length: $\bar{l}_\text{g} = 79.8\,\mu\text{m}$. Porosity obtained from the image is 40.7 %.

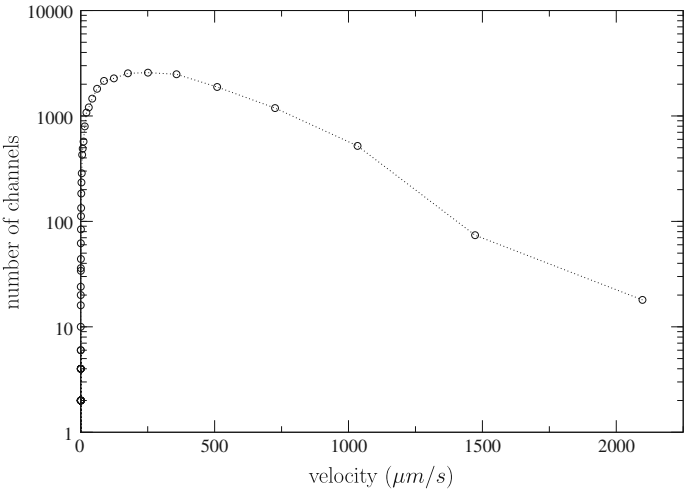

Fig. 3 Velocity-field distribution in the pore network having the typically log-normal distribution observed in sands or sandstones (Manwart et al. 2002)

Flow-field Computation Flow is simulated by applying a macroscopic pressure difference ΔP across the network. The local flow rate between the pore i and the neighbouring pore j is defined by Poiseuille's law (Poiseuille 1840a,b)

$$q_{ij} = \frac{\pi d_{ij}^4}{128 \mu l_{ij}} (P_i - P_j) \tag{3}$$

where l_{ij} is the length of the channel ij, d_{ij} its diameter, P_i (P_j) the pressure in the pore i (j) and μ the viscosity of the fluid. In each pore mass conservation is imposed. The problem is reduced to a system of linear algebraic equations, the solution of which gives the pressure in the pores.

Periodic boundary conditions on the lateral faces were used. To this goal we applied a diluted Delaunay triangulation algorithm (Bauer et al. 2011) between the nodes of two opposite borders in order to create new channels across the periodic boundaries. As 3D Delaunay triangulation leads to very high coordination numbers, channels are then removed until the coordination number distribution matches the one of the initial network. Diameters and lengths of the new channels were randomly chosen using the channel-size distribution of the network.

Figure 3 shows the velocity field distribution. It has the typically log-normal distribution observed in sands or sandstones (Manwart et al. 2002).

3.2 Transport of Walkers

We suppose passive walkers standing for the water molecules whose displacements are measured by NMR. At time $t = 0$ walkers are injected in all channels. The number of walkers injected in a channel depend on its volume and the volume of its appertaining nodes. Walkers are then displaced in the channels of the network.

Transport in the Channel Walkers are displaced in each channel on the line connecting node i and node j by convection and diffusion. At each time step d_t the walker jumps first according to the mean velocity in the channel and second by an instantaneous diffusive

jump. A random Normal law (Gaussian distribution) consistent with the effective molecular diffusion coefficient of each channel gives the length of the diffusive jump. We suppose that walker transport reaches an asymptotic regime in the channels following Taylor dispersion (Taylor 1954). Particle positions $\mathbf{X}(t + d_t)$ at the instant $t + d_t$ can then be determined from

$$\mathbf{X}(t + d_t) = \mathbf{X}(t) + v_{\text{mean},ij} d_t \mathbf{e} + \sqrt{2 D_{\text{eff},ij} d_t} N \mathbf{e} \tag{4}$$

where $v_{\text{mean},ij}$ is the mean velocity of channel ij. $D_{\text{eff},ij}$ is its effective diffusion coefficient given by $D_{\text{eff},ij} = D_{\text{m}}(1 + Pe_{ij}^2/192)$, where Pe_{ij} is the local Peclet number of the channel ij. $\mathbf{e}$ is a unit vector in the flow direction of the channel ij. N is a random variable distributed by a standard centred normal law (Box and Muller 1950). We verified, that results do not depend on whether the diffusive jump is performed before or after the convective step.

Node Transition When a walker reaches a network node, a new channel has to be selected. Walkers can pass a node during the advective or the diffusive step. The next channel is chosen according to rules that depend on the type of the current step. If the walker passes the node during the advective step, the probability of a channel to be selected is linearly proportional to its mean flow rate. Moreover, only out-flowing channels can be chosen. In contrast to that, if a walker passes a node during the diffusive step all channels connected to this node can be chosen, except the channel in which the walker arrives. In this case, the probability of a channel to be chosen is proportional to its cross-sectional area. In both cases (advective and diffusive step) probability distributions to choose the next channel are normal. This transition law has already been proposed several times in literature and simulates complete mixing in the nodes (Imdakm and Sahimi 1991; Park et al. 2001; Bijeljic et al. 2004; Rhodes and Blunt 2006).

Number of Injected Walkers and Time Step Definition Simulations are performed with $N_{\text{b}} = 50,000$ walkers, above this number propagators become independent of N_{b}. The time step d_t was chosen in a way that the largest distance that a walker might cover by advection and diffusion during one time step is smaller than the shortest channel (Press et al. 2007). It can be computed from

$$L_{\min} = v_{\max} d_t + \sqrt{2 D_{\text{eff},\max} d_t} \tag{5}$$

where $L_{\min}$ is the length of the shortest channel, $v_{\max}$ the highest velocity found in the entire network and $D_{\text{eff},\max}$ the highest local effective diffusion coefficient.

Re-injection of Walkers As walkers are injected everywhere in the network in order to simulate the water presence in the entire porous medium, it is important to allow walkers leaving the network at the outlet to reenter at the inlet. To achieve incompressibility, each walker, that leaves the network must be re-injected, at an inlet node. To choose the latter automatically, inlet and outlet nodes are connected by a Delaunay triangulation algorithm. A walker leaving the network at an outlet node is then directly re-injected at an inlet node connected to the latter by the triangulation algorithm. The inlet node is chosen randomly following a uniform distribution.

Computation of the Numerical Propagator The numerical propagator corresponds to a displacement histogram. Displacement of a particle during the observation time $t_\Delta = t_2 - t_1$ in a specific direction (e.g., x) is computed from

$$\Delta X(t_\Delta) = (x(t_2) + L N_r(t_2)) - (x(t_1) + L N_{\text{r}}(t_1)) \tag{6}$$

where L is the network length and N_{r} the number of recirculations. Minimal and maximal values of the histogram are given by the smallest and largest value of $\Delta X(t_\Delta)$, 100 classes of identical width are used.

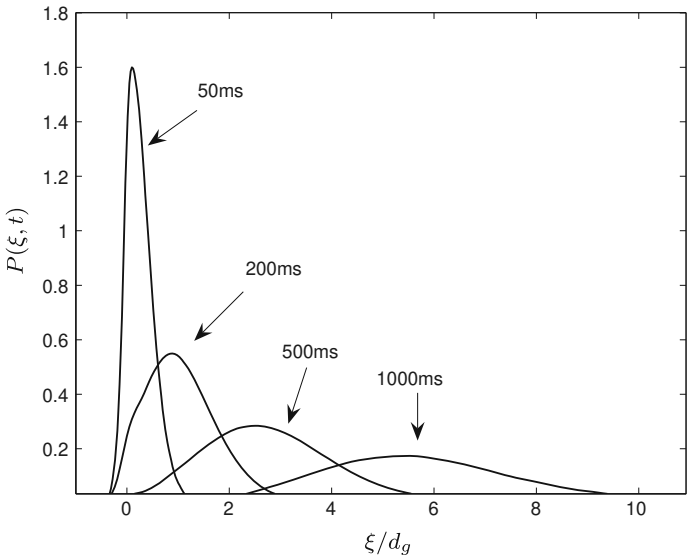

Fig. 4 Propagators measured by NMR for different observation times (flow rate: 250 ml/h, ξ: displacement, d_g: average grain size). For small observation times propagators show a significant asymmetric shape close to a log-normal distribution as the asymptotic regime is not reached yet. For longer observation times where mechanical mixing dominates, NMR propagators are a signature of dispersion and show in this simple case a quasi-Gaussian shape

4 Results

4.1 NMR Propagators

Molecular displacements were measured by NMR for different observation times (t_Δ = 50, 200, 500, 1000 ms) and flow rates (50, 250, 500 ml/h) (see Fig. 4 for the flow rate of 250 ml/h). As can be seen, for small observation times propagators show a significant asymmetric shape close to a log-normal distribution. This is a signature of the transition from a preasymptotic to an asymptotic regime, as described in Scheven and Sen (2002) and Guillon et al. (2013). Indeed, for small observation times the NMR propagator reproduces the characteristics of the velocity field around the grains with some influence of diffusion. For longer observation times, where mechanical mixing dominates, NMR propagators are a signature of dispersion and show in this simple case a quasi-Gaussian shape, however, small deviations from the Gaussian curve can be observed (Guillon et al. 2013). When focusing on the variance of the water molecule displacements as a function of time for the different flow rates (Fig. 5), we see a piece-wise linear time dependency on a log–log scale. Variance satisfies $\sigma^2 \propto t^\alpha$, where α defines the dispersion regime ($\alpha = 1$, normal dispersion, $\alpha > 1$ superdispersion). We computed α from the slope between t_Δ =200 ms and t_Δ =1000 ms and obtained $\alpha =$ 1.03 (50 ml/h), $\alpha = 1.19$ (250 ml/h), and $\alpha = 1.19$ (500 ml/h). Thus, depending on the flow rate, dispersion may be normal ($\alpha \approx 1$) or super-dispersive ($\alpha = 1.19$). In order to check that the observed super-dispersion is not a transient phenomena, a more general approach is to plot $\sigma/ < \xi >$ as function of $<\xi>/d_g$ where $< \xi >$ is the mean displacement and d_g the average grain size (see Fig. 6). The asymptotic regime is reached when the curves $\sigma/< \xi >= f(<\xi>/d_g)$ collapse for different flow rates (Guillon et al. 2013). As can be seen,

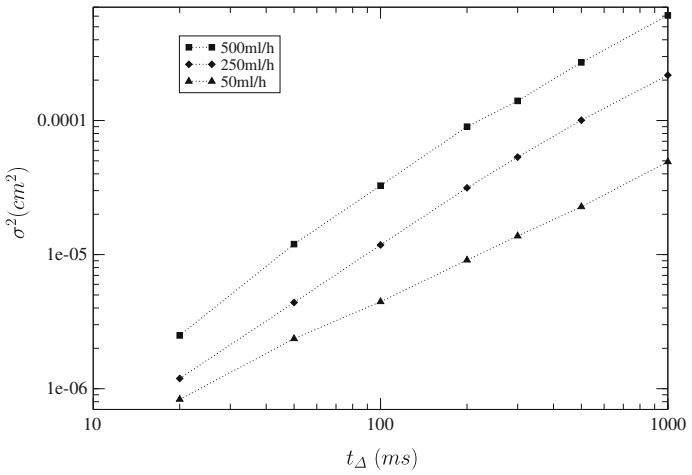

Fig. 5 Variance of the displacement as a function of the observation time t_Δ for different flow rates. Depending on the flow rate, dispersion may be normal ($\alpha \approx 1$ for (50 ml/h)) or super-dispersive ($\alpha = 1.19$ for (250 ml/h) and (500 ml/h))

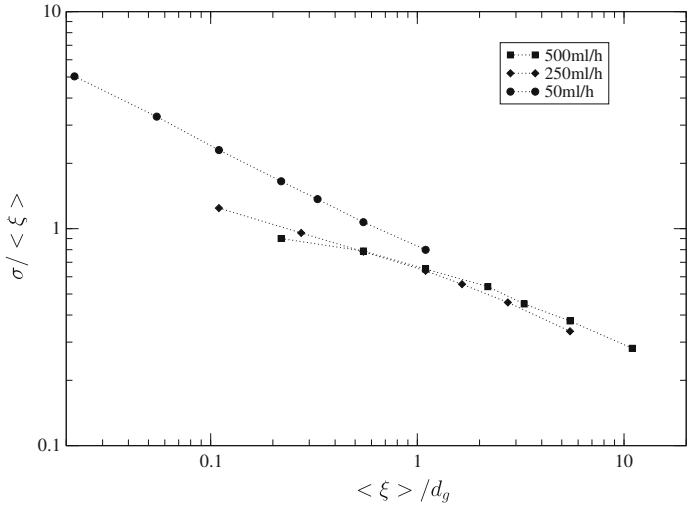

Fig. 6 Asymptotic behavior of the water molecule displacements. d_g is the grain size and $< \xi >$ the mean displacement. The asymptotic regime is reached when the curves $\sigma/ < \xi >= f(< \xi > /d_g)$ collapse for different flow rates (Guillon et al. 2013)

the system reaches the asymptotic limit for large observation times. Nevertheless, in this case NMR allows observing the asymptotic regime only during a very short time interval. Thus, PNM simulations of the experimental propagators are expected to provide useful information on grain packings by extending the NMR observation times to larger values.

4.2 PNM Propagators

The average velocity and the molecular diffusion coefficient D_m in the PNM were chosen in a way that they were identical to those of the NMR experiment performed with a flow rate

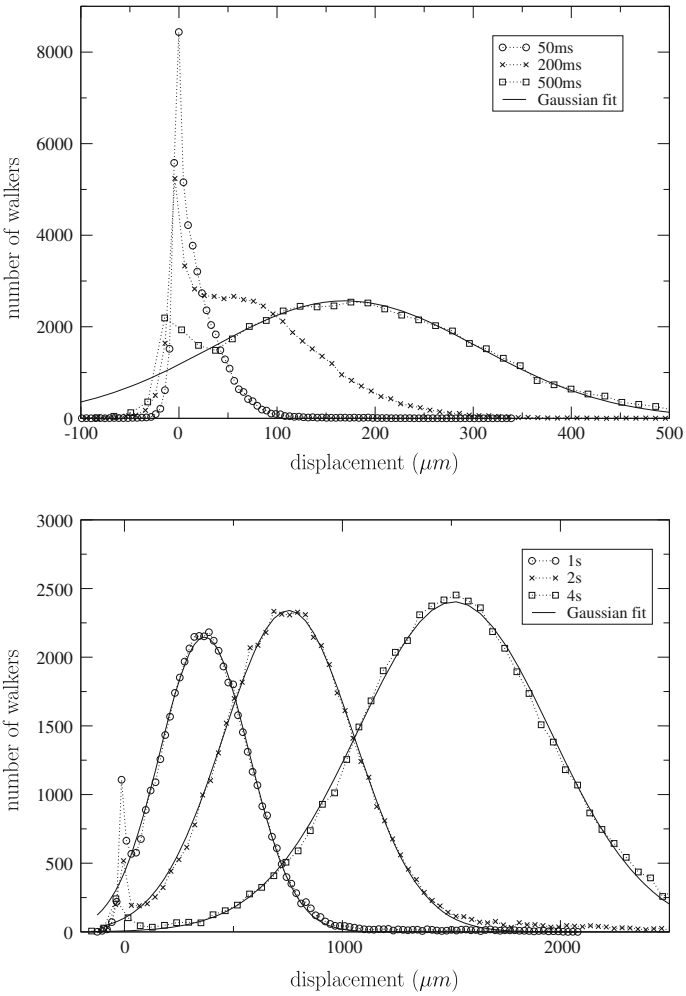

Fig. 7 Evolution of the numerical propagator of the sand as a function of time as well as the according Gaussian fit. Propagator shapes are approximately similar to those observed by NMR. However, for intermediate observation times the numerical propagators show a significant peak caused by stagnant walkers (zero-displacement) that is not observed in our experiments

of 250 ml/h. Thus, experiments and simulation have the same Peclet number (the grain size is identical).

For the sand considered and similarly to experiments, the shape of the numerical propagators is likely to follow a log-normal distribution for small t_Δ whereas it becomes close to a Gaussian curve for larger t_Δ (see Fig. 7 for the observation times t_Δ : 50, 200, 500, 1000 ms, 4 s). Hence, propagator shapes are approximately similar to those observed by NMR. However, for intermediate observation times the numerical propagators show a significant peak caused by stagnant walkers (zero-displacement), that is not observed in our experiments. The aim of the following discussion is to provide an explanation of the origin of the peak based on the network structure and on the detailed history of each walker, an information available in simulations.

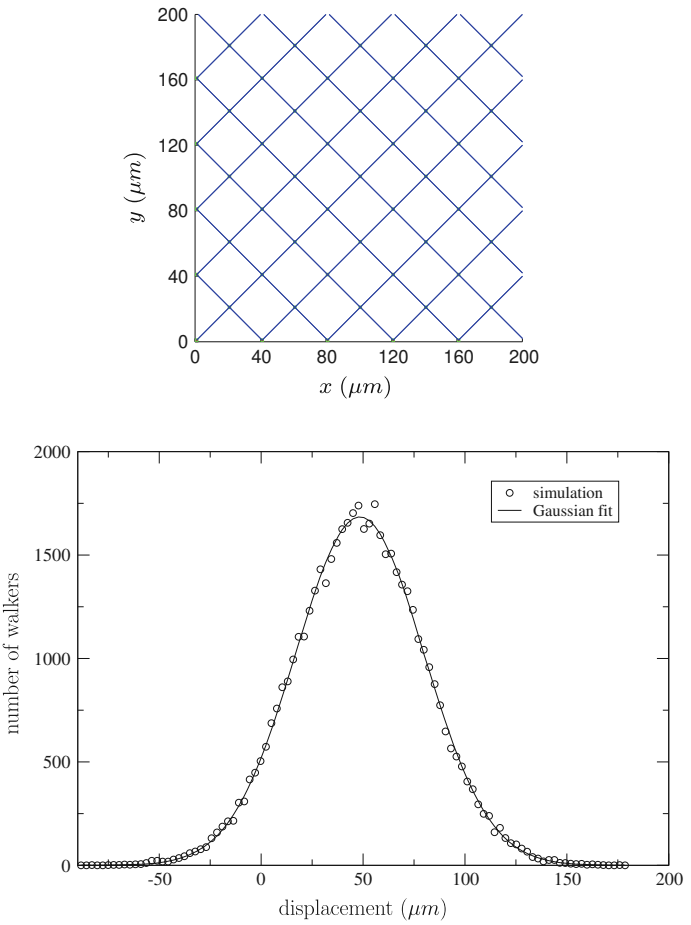

Fig. 8 *Top* 2D rectangular network with a 45° orientation, *bottom* propagator of the rectangular network for an observation time t_Δ =400 ms that does not present a peak caused by stagnant walkers

The network exhibits very few pores (35) connected to only one single pore, so-called dead-ends. We verified that such an important peak cannot be caused solely by stagnation in dead-ends. Now, careful inspection of each trajectory shows, that even though stagnant walkers are in low velocity zones, channels whose direction is more or less orthogonal to the mean flow play a particular role. This agrees with the results presented by Damion et al. (2000) and Lebon et al. (1997). Damion et al. (2000) simulated propagators in a distorted cubic network with an initial angle between the channels of 90°. In order to distort the network, node positions were displaced. For weak distortion, stagnant peaks were observed in the propagators. Also, Lebon et al. (1997) observed a stagnant peak in their simulations. Identically, they argue that the stagnant peak is partially due to transverse channels. Following these references, we first simulate propagators of a 2D rectangular network oriented at 45° (Fig. 8, top, 5000 pores, channel length: $l = 20\sqrt{2}$ µm, total network length: $L = 2,000$ µm). This type of network does not contain orthogonal channels and its propagator does not present a stagnant peak (Fig. 8, bottom). We can therefore conclude that particularly orthogonal channels lead to the stagnant peak. Indeed, the network restricts the ensemble of possible walker trajectories in

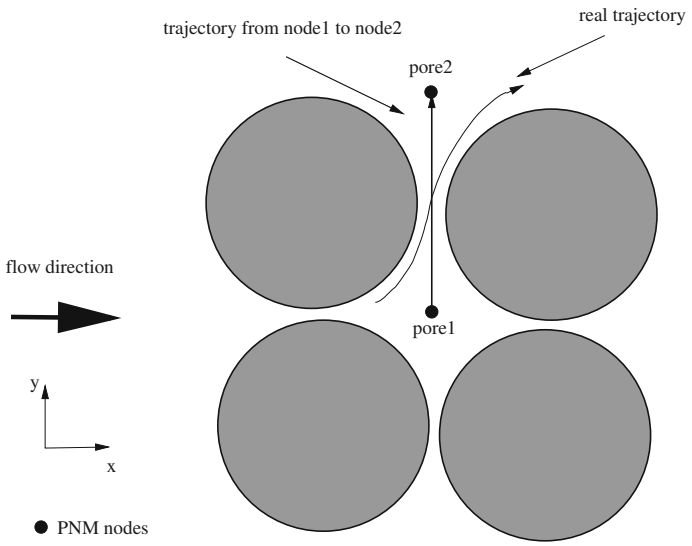

Fig. 9 Particle trajectory of the pore network in comparasion to the trajectory in the real porous medium. In this situation, the walker trajectory is limited by the pore network structure. The pore network does not allow the correct representation of the real trajectory

comparison to the real trajectories. Figure 9 shows an explicit situation where the simplified network geometry limits the walker displacements. Whereas walkers moving from pore1 to pore2 on the real trajectory contribute to the propagator with a $\Delta x \neq 0$, walkers moving from node1 to node2 in the PNM contribute with a very small Δx ($\Delta x \sim 0$) as they move only on the line connecting the nodes. This significantly diminishes walker displacements, and enhances the stagnant peak. In addition, transverse diffusion was neglected. Thus, the model does not allow the simulation of the real lateral positions of the walkers in the channels. In order to compensate the artificial tapering of the displacements, we add a small displacement δ to the x coordinate of the final position of each walker depending on the angle ϕ between the channel in which the walker is situated and the macroscopic flow direction (x direction). The new position is given by

$$x'(t_{\text{final}}) = x(t_{\text{final}}) + \delta W_n(1 - \cos\phi) \tag{7}$$

where W_n are random numbers, either uniformly distributed in $[-1; 1]$ or following a Gaussian distribution with zero mean and unit variance. δ is set to $D/2$, d or $d/2$, where d is the channel diameter in which the particle is situated and D the mean diameter of the pores inclosing this channel. Figure 10 shows that in all cases the peak is reduced without changing the entire propagator. Best results were obtained for $\delta = D/2$ with W_n given by a Gaussian distribution. Thus, displacements perpendicular to the channel direction cannot be neglected and should be included in the simulation, if the entire walker displacement distribution is of interest.

Figure 11 shows the evolution of the propagator as a function of time taking into account the lateral position of the walkers in the channel (we set $\delta = D/2$ and W_n follows a Gaussian distribution). It can be seen that for observation times larger than 200 ms the stagnant peak disappears and the propagators become similar to those experimentally observed. For small t_Δ, small inconsistencies can be observed, although the shape is still relatively similar to the

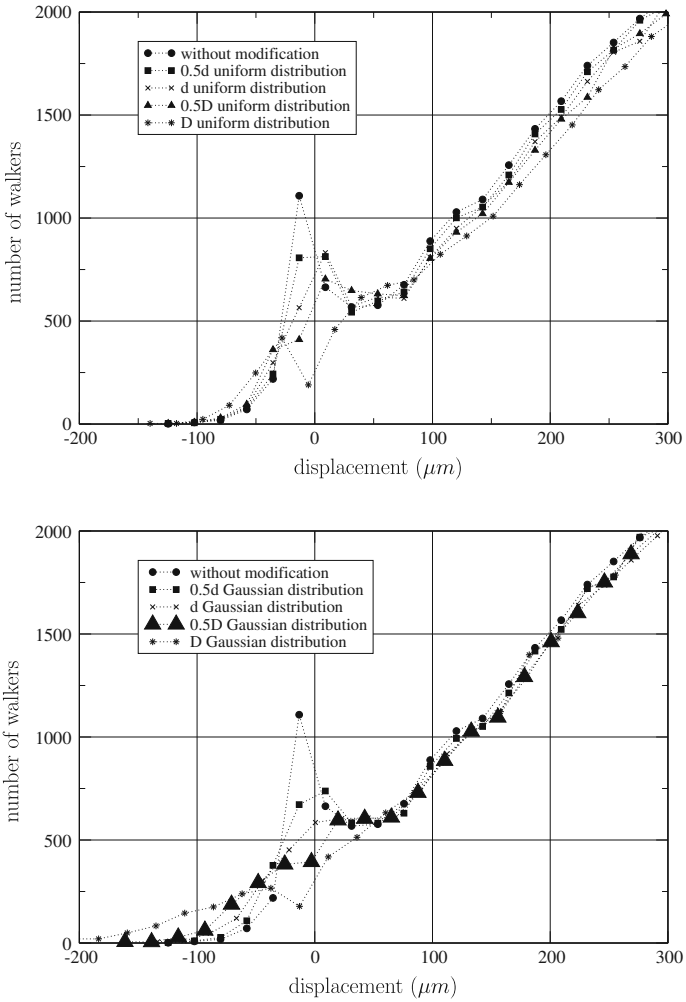

Fig. 10 Propagators before and after the consideration of the lateral walker position in the channel for an observation time t_Δ =1 s. The lateral position is distributed by a uniform and a Gaussian random distribution having different maximal values (uniform distribution) or standard-deviations (Gaussian distribution). The stagnant peak is quasi eliminated for $\delta = D/2$

experimental propagator. Thus, when simulating propagators for large t_Δ the lateral position of the walkers in the channel can be statistically approximated by a Gaussian distribution, whereas it is necessary to know its exact position when simulating propagators for small t_Δ.

Considering the variance of the walker displacement distribution generally used to compute the dispersion coefficient, it is only slightly influenced by the peak and the choice of δ (see Table 1). Thus, in order to determine the dispersion coefficient it is not necessary to take into account the real lateral position of the walkers.

4.3 Asymptotic Behaviour

Figure 12 shows the normalized variance σ^2/σ^2 (50 ms) as a function of time, based on either the numerical or the experimental propagators. Although numerical values of σ^2 are

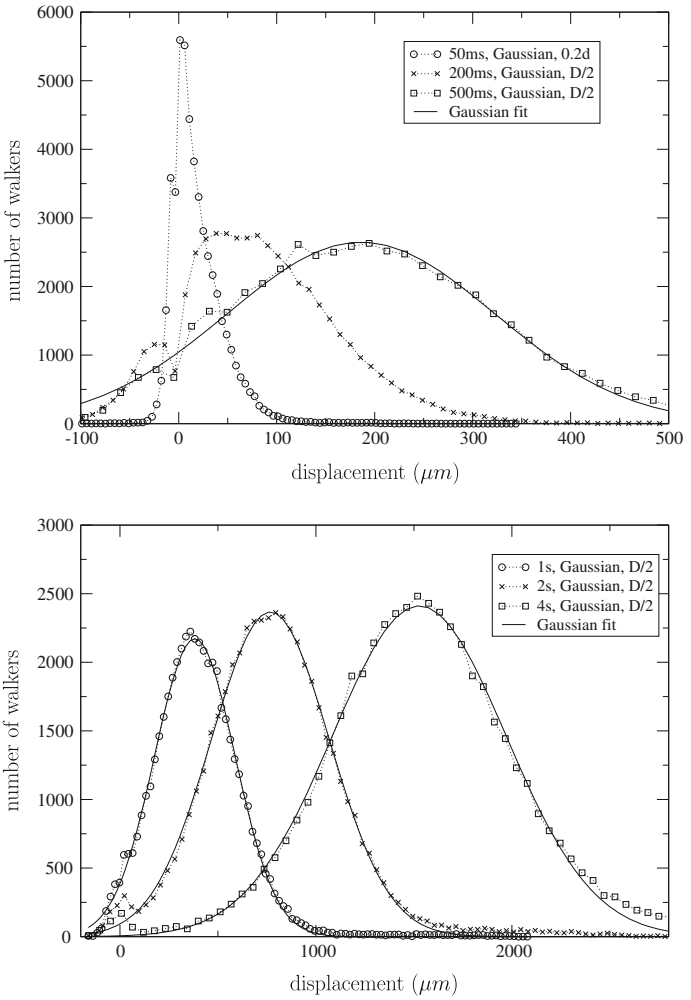

Fig. 11 Propagators after the consideration of the lateral walker position in the channel for different observation times. The lateral position is randomly distributed by a Gaussian distribution with standard deviation $D/2$. For observation times larger than 200 ms the stagnant peak disappears and the propagators become similar to those experimentally observed

Table 1 Variance of the walker displacement as a function of the distribution type of the lateral position of the walkers in the channels normalized by the variance obtained before modification of the lateral position

	Uniform distribution	Gaussian distribution
0.5	1.004	1.005
d	1.009	1.014
$0.5D$	1.009	1.019
D	1.028	1.066

slightly higher than the experimental values, the asymptotic limits are very close ($\alpha_{\mathrm{PNM}} = 1.22$, $\alpha_{\mathrm{NMR}} = 1.19$, the slope was computed from the last 4 (NMR) or 5 (PNM) data points). NMR and PNM both detect a slightly super-dispersive behaviour. This allows us

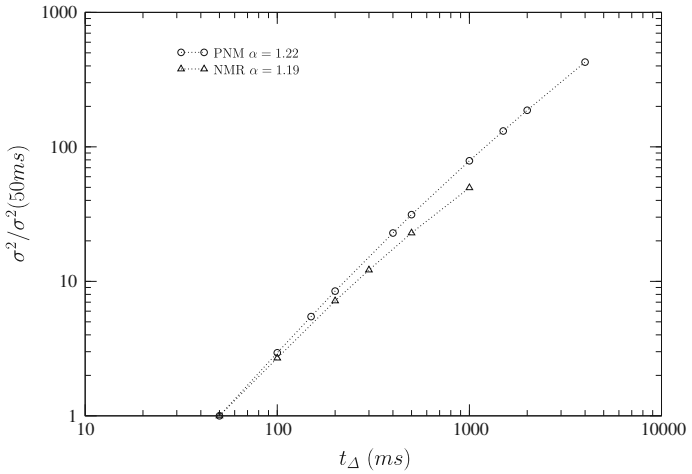

Fig. 12 Normalized variance σ^2/σ^2 (50 ms) as a function of the observation time t_Δ of both numerical and experimental propagators. Both NMR and PNM detect a slightly super-dispersive behavior

to draw conclusions on the origin of the dispersion behaviour. Indeed, as we have already mentioned in the introduction, PNM is based on a simplified representation of the pore space taking into account the topology and specific geometrical characteristics of the porous media (e.g., connectivity, channel-size distribution). However, small scale characteristics as the particular grain shape or the surface roughness are not considered. Thus, the fact that PNM correctly reproduces the dispersion type shows that the topological and geometrical meso-scale characteristics induce the non-Gaussian dispersion.

Simulating the Longtime Behaviour of NMR Propagators We have seen that the random walk pore network model allowed the simulation of the asymptotic behaviour measured by NMR on a particular sand pack. As experimental and numerical results are in good accordance, we can conclude that the model can predict the longtime behaviour of other type of media, where the asymptotic limit cannot be reached by NMR.

5 Conclusion

We simulated displacement distributions of water molecules in Fontainebleau sand using a pore network model combined with a random walk algorithm and compared them to propagators obtained by NMR. For high observation times, the propagator shape was quasi-Gaussian. However, for lower observation times they presented a peak close to zero displacement, that was not experimentally observed. We attribute this peak to channels directed orthogonally to the flow direction. In the pore network walkers move from one pore to the next pore on the line connecting the barycenters of the pores, neglecting lateral displacements inside a channel. Thus, the displacement in the flow direction might become very small in these channels. We therefore proposed to add a small random displacement to the x coordinate of the final position of each walker depending on the angle between the channel in which the walker is situated and the macroscopic flow direction. In this way, we could model the lateral position of the walker and simulation results were improved.

From the displacement distributions we computed the variance in order to determine the dispersion regime. Very good agreement of the time evolution of the numerical variance with

the experimental data was found, staying for the quality of the model as it is not based on any adjustable parameters. Both, experimental and numerical time evolution of the variance show a slightly super-dispersive behaviour ($\alpha_{\mathrm{NMR}} = 1.19$ and $\alpha_{\mathrm{PNM}} = 1.22$). We explained this anomalous dispersion by the following fact. As the model results are in good accordance with the experimental data, although pore network models do not take into account small scale features of the porous medium (e.g., surface roughness), the origin of the super-dispersion can be attributed to the topology and geometry of the porous medium.

As experimental and numerical results are in good accordance, we can conclude that the model can predict the longtime behaviour of other type of media, where the asymptotic limit cannot be reached by NMR.

Acknowledgments The authors have been supported by Agence Nationale de la Recherche (ANR Project No. ANR-09-SYSC-015). We thank also C. Latrille (CEA) for providing the Fontainebleau sand and S. Youssef (IFPEN) for the network generation.

References

Bauer, D., Youssef, S., Han, M., Bekri S. Rosenberg, E., Fleury, M., Vizika, O.: From computed microtomography images to resistivity index calculations of heterogeneous carbonates using a dual-porosity pore-network approach: influence of percolation on the electrical transport properties. Phys. Rev. E **84**(1 Pt 1), 011133 (2011)

Benson, D., Wheatcraft, S., Meerschaert, M.: Application of fractional advection–dispersion equation. Water Resour. Res. **36**, 1403–1412 (2000)

Bijeljic, B., Mostaghimi, P., Blunt, M.: Insights into non-Fickian solute transport in carbonates. Water Resour. Res. **49**, 1–15 (2013a)

Bijeljic, B., Muggeridge, A.H., Blunt, M.J.: Pore-scale modeling of longitudinal dispersion. Water Resour. Res. **40**, 1–9 (2004)

Bijeljic, B., Raeini, A., Mostaghimi, P., Blunt, M.: Predictions of non-Fickian solute transport in different classes of porous media using direct simulation on pore-scale images. Phys. Rev. E **87**(1), 013011 (2013b)

Blunt, M.: Flow in porous media: pore-network models and multiphase flow. Curr. Opin. Colloid Interface Sci. **6**, 197–207 (2001)

Bodin, J., Porel, G., Delay, F., Ubertosi, F., Bernard, S., de Dreuzy, J.R.: Simulation and analysis of solute transport in 2D fracture/pipe networks: the SOLFRAC program. J. Contam. Hydrol. **89**, 1–28 (2007)

Box, G.E.P., Muller, M.E.: A note on the generation of random normal deviates. Annal. Math. Stat. **21**, 455 (1950)

Damion, R.A., Packer, K.J., Sorbie, K.S., McDougall, S.R.: Pore-scale network modelling of flow propagators derived from pulsed magnetic field gradient spin echo NMR measurements in porous media. Chem. Eng. Sci. **55**, 5981–5998 (2000)

Guillon, V., Fleury, M., Bauer, D., Néel, M.C.: Super-dispersion in homogeneous unsaturated porous media using NMR propagators. Phys. Rev. E **87**, 043007 (2013)

Imdakm, A., Sahimi, M.: Computer simulation of particle transport processes in flow through porous media. Chem. Eng. Sci. **46**, 1977–1993 (1991)

Koehne, M., Schlueter, S., Vogel, H.J.: Predicting solute transport in structured soil using pore network models. Vadose Zone J. **10**, 1082–1096 (2011)

Lebon, L., Leblond, J., Hulin, J.P.: Experimental measurement of dispersion processes at short times using a pulsed field gradient NMR technique. Phys. Fluids **9**, 481–490 (1997)

Lebon, L., Oger, L., Leblond, J., Hulin, J.P., Martys, N.S., Schwartz, L.M.: Pulsed gradient NMR measurements and numerical simulation of flow velocity distribution in sphere packings. Phys. Fluids **8**, 293–301 (1996)

Levy, M., Berkowitz, B.: Measurement and analysis of non-Fickian dispersion in heterogeneous porous media. J. Contam. Hydrol. **64**, 203–226 (2003)

Li, Y., Farrher, G., Kimmich, R.: Sub- and superdiffusive molecular displacement laws in disordered porous media probed by nuclear magnetic resonance. Phys. Rev. E **74**, 066309 (2006)

Manwart, C., Aaltosalmi, U., Koponen, A., Hilfer, R., Timonen, J.: Lattice-Boltzmann and finite-difference simulations for the permeability for three-dimensional porous media. Phys. Rev. E **66**, 016702 (2002)

Manz, B., Gladden, L.F., Warren, P.B.: Flow and dispersion in porous media: Lattice–Boltzmann and NMR studies. AIChE J. **45**, 1845–1854 (1999)

Metzler, R., Klafter, J.: The random walks guide to anomalous diffusion : a fractional dynamics approach. Phys. Rep. **339**, 1–77 (2000)
Padilla, I., Yeh, T.C., Conklin, M.: The effect of water content on solute transport in unsaturated porous media. Water Resour. Res. **35**, 3303–3313 (1999)
Park, Y.J., de Dreuzy, J.R., Lee, K.L.: Transport and intersection mixing in random fracture networks with power law length distribution. Water Resour. Res. **37**, 2493–2501 (2001)
Poiseuille, J.: Recherches expérimentales sur le mouvement des liquides dans les tubes de très petits diamètres (1840a)
Poiseuille, J.: Recherches expérimentales sur le mouvement des liquides dans les tubes de très petits diamètres (1840b)
Press, W.H., Teukolsky, S.A., Vetterling, W.T., Flannery, B.P.: Numerical Recipes in C: The Art of Scientific Computing, 3rd edn. Cambridge University Press, Cambridge (2007)
Pudney, C.: Distance-ordered homotopic thinning: a skeletonization algorithm for 3D digital images. Comput. Vis. Image Underst. **72**, 404–413 (1998)
Rhodes, M.E., Blunt, M.: An exact particle tracking algorithm for advective–dispersive transport in networks with complete mixing at nodes. Water Resour. Res. **42**, 1–7 (2006)
Sahimi, M.: Flow and Transport in Porous Media and Fractured Rock: From Classical Methods to Modern Approaches, 2nd edn. VCH, Weinheim (2011)
Sahimi, M., Heiba, A.A., Davis, H.T., Scriven, L.E.: Dispersion in flow through porous-media. 2. Two-phase flow. Chem. Eng. Sci. **41**, 2123–2136 (1986)
Scheven, U.M., Harris, R., Johns, M.L.: Quasi-asymptotic dispersion. Magn. Resonance Porous Media **1081**, 18–21 (2008)
Scheven, U.M., Harris, R., Johns, M.L., Gladden, L.: Quantitative nuclear magnetic resonance measurements of preasymptotic dispersion in flow through porous media. Phys. Fluids **17**, 117107 (2005)
Scheven, U.M., Sen, P.N.: Spatial and temporal coarse graining for dispersion in randomly packed spheres. Phys. Rev. Lett. **89** (2002)
Seymour, J.D., Callaghan, P.T.: Generalized approach to NMR analysis of flow and dispersion in porous media. AIChE J. **43**, 2096–2111 (1997)
Taylor, G.: The dispersion of matter in turbulent flow through a pipe. Proc. R. Soc. Lond. Ser A. Math. Phys. Sci. **223**, 446–468 (1954)
Tessier, J.J., Packer, K.J., Thovert, J.F., Adler, P.M.: NMR measurements and numerical simulation of fluid transport in porous solids. AIChE J. **43**, 1653–1661 (1997)
Zhao, W.S., Picard, G., Leu, G., Singer, P.M.: Characterization of single-phase flow through carbonate rocks: quantitative comparison of NMR flow propagator measurements with a realistic pore network model. Transp. Porous Media **81**, 305–315 (2010)